

NLO production of HH, ZH, and ZZ by gluon fusion, in the high-energy limit

Joshua Davies^{a,*}

^a*Department of Physics and Astronomy, University of Sussex, Brighton, BN1 9QH, UK*

E-mail: j.o.davies@sussex.ac.uk

In this talk we discuss computations of NLO virtual corrections to four-point gluon-fusion processes; in particular the production of HH, ZH and ZZ. Recently these processes have been computed numerically, but they are not known analytically. We will discuss how one can perform an expansion of these amplitudes in the high-energy limit, and improve the resulting series through the use of Padé approximants.

*** *The European Physical Society Conference on High Energy Physics (EPS-HEP2021)*, ***

*** *26-30 July 2021* ***

*** *Online conference, jointly organized by Universität Hamburg and the research center DESY* ***

*Speaker

1. Introduction

A good theoretical understanding of $2 \rightarrow 2$ gluon fusion processes is important for a wide variety of on-going studies at the Large Hadron Collider (LHC). Such processes include the dominant production mode for Higgs boson pairs, as well as forming an important contribution to backgrounds for Higgs boson decays. In these proceedings we consider, in particular, the production of HH , ZZ and ZH final states in gluon fusion. At leading order (LO), which corresponds to one loop, exact expressions have been known for these amplitudes for a long time [1–6]. At next-to-leading order (NLO), however, exact analytic expressions are still unknown some thirty years later, due to the complexity of $2 \rightarrow 2$ Feynman integrals with massive external legs and internally propagating particles.

Nonetheless, there have been great efforts to understand the NLO amplitudes through the use of numerical evaluation [7, 8] or various expansions, including the large- m_t limit [9–12], around the top quark threshold [13, 14] and for small transverse momenta [15, 16]. The topic of these proceedings is an expansion in the high-energy region [17–19], in which numerical evaluations are very expensive and other expansions do not converge.

These proceedings are organised as follows: in Section 2 some notation and definitions will be given and in Section 3 we describe how the high-energy expansion is computed. In Section 4, we discuss a method by which the high-energy expansion can be further improved by Padé approximants, in order to expand the kinematic region which can be described.

2. Notation and Setup

The amplitudes for $gg \rightarrow HH$, $gg \rightarrow ZZ$ and $gg \rightarrow ZH$ can be written as linear combinations of Lorentz structures and so-called “form factors”. The number of structures depends on the processes; for the HH , ZZ and ZH final states we define 2, 18 and 6 form factors, respectively:

$$\mathcal{M}_{gg \rightarrow HH}^{\mu\nu} = \sum_{i=1}^2 A_i^{\mu\nu} F_i, \quad \mathcal{M}_{gg \rightarrow ZZ}^{\mu\nu\rho\sigma} = \sum_{i=1}^{18} A_i^{\mu\nu\rho\sigma} F_i, \quad \mathcal{M}_{gg \rightarrow ZH}^{\mu\nu\rho} = \sum_{i=1}^6 A_i^{\mu\nu\rho} F_i, \quad (1)$$

where the A_i and F_i are, of course, specific to each process. The form factors are computed by projecting them out of the amplitude with projectors P_i such that, e.g., $P_{i,\mu\nu} \mathcal{M}_{gg \rightarrow HH}^{\mu\nu} = F_i$. The form factors are functions of the final-state particle masses and the Mandelstam variables $s = (q_1 + q_2)^2$, $t = (q_1 + q_3)^2$ and $u = (q_2 + q_3)^2$ where q_1, q_2 are the momenta of the incoming gluons and $q_3, q_4 = -q_1 - q_2 - q_3$ are the momenta of the final-state particles. We have that $q_1^2 = q_2^2 = 0$ but q_3^2 and q_4^2 depend on which process is being considered.

Once the form factors have been computed and ultra-violet renormalized, infra-red divergences remain at NLO. These are removed by a subtraction procedure

$$F_i^{\text{NLO}} = F_i^{\text{NLO,UV-ren}} - K_g^{(1)} F_i^{\text{LO}}, \quad (2)$$

where $K_g^{(1)}$ can be found in Ref. [20]. In terms of these infra-red subtracted form factors, we construct “virtual-finite cross sections”, which take the form

$$\mathcal{V}_{\text{fin}}^{\text{NLO}} \sim \left(\frac{C_A}{2} \pi^2 - \frac{C_A}{2} \log^2 \frac{\mu^2}{s} \right) \left(\sum_i |F_i^{\text{LO}}|^2 \right) + \sum_i \left(F_i^{\text{LO}*} F_i^{\text{NLO}} + F_i^{\text{LO}} F_i^{\text{NLO}*} \right), \quad (3)$$

up to overall constants. We will later compare the high-energy expansion of these virtual-finite cross sections to evaluations by numerical methods in Fig. 4.

3. High-Energy Expansion

Having introduced the general setup and notation, we now discuss how the high-energy expansion of the form factors can be computed. We start by generating the Feynman diagrams for the amplitude of interest with `qgraf` [21]. The programs `q2e` and `exp` [22, 23] are then used to convert the output to a suitable notation and match the diagrams to a set of $2 \rightarrow 2$ integral topologies. The result is a set of diagram files which are processed by `FORM` [24], which applies the Lorentz projectors for the form factors discussed in Section 2, computes traces and colour factors (using `COLOR` [25]), finally writing each diagram as a linear combination of scalar Feynman integrals.

At this point, the Feynman integrals depend on many parameters, including the masses of the final-state particles: $I(\{m_Z^2, m_H^2\}, m_t^2, s, t, \epsilon)$. Since we are interested in the high-energy limit of the form factors, we assume that $\{m_Z^2, m_H^2\} < m_t^2 \ll s, t$. Therefore, we can Taylor expand the integrals and their coefficients for $\{m_Z^2, m_H^2\} \rightarrow 0$, leaving integrals which no longer depend on the final-state particle masses, for example,

$$I(m_H^2, \dots) = I(0, \dots) + m_H^2 \frac{d}{dm_H^2} I(0, \dots) + O(m_H^4). \quad (4)$$

We can now perform an integration-by-parts (IBP) reduction using `FIRE` [26] to obtain the form factors in terms of a linear combination of a set of master integrals $\vec{J}(m_t^2, s, t, \epsilon)$. The expansion of Eq. (4) means that the IBP coefficients do not depend on m_H or m_Z , making the reduction significantly easier. The resulting set of master integrals is suitable to describe $gg \rightarrow HH$, $gg \rightarrow ZZ$ and $gg \rightarrow ZH$ as well as, for example, $gg \rightarrow \gamma\gamma$ or $gg \rightarrow Z\gamma$. Only the details of the expansion of Eq. (4) differ between the processes.

The next step is to perform an expansion of the master integrals, assuming that $m_t^2 \ll s, t$. This can be performed efficiently by making use of differential equations for the master integrals. Differentiating each master integral w.r.t. m_t^2 and IBP reducing the result leads to a coupled system of equations of the form

$$\frac{d}{dm_t^2} \vec{J} = M(m_t^2, s, t, \epsilon) \cdot \vec{J}, \quad (5)$$

where the matrix M encodes the m_t dependence of each J_a of \vec{J} . By substituting a series ansatz for the master integrals,

$$J_a = \sum_i \sum_j \sum_k C_{a,ijk}(s, t) \epsilon^i (m_t^2)^j \log^k(m_t^2), \quad (6)$$

into Eq. (5) we obtain a system of *linear* equations for the coefficients $C_{a,ijk}$. By supplying some boundary values for the system (i.e. values for $C_{a,ijk}$ at leading i, j, k —see Ref. [27] for a detailed discussion of their evaluation) the system can be solved order-by-order in i, j, k to obtain a deep expansion of each J_a in powers of m_t^2 .

Fig. 1 shows the effect of expanding to various orders in m_H^2 and m_Z^2 , for the leading-order $gg \rightarrow HH$ and $gg \rightarrow ZZ$ differential cross sections, respectively. In both cases, the curves

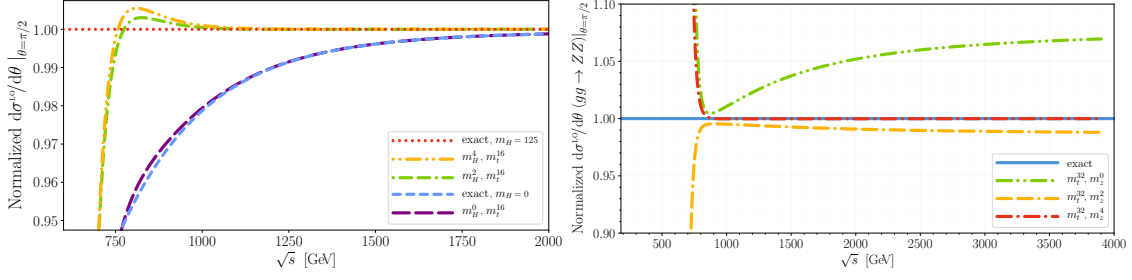


Figure 1: High-energy expansions of leading-order differential cross sections for $gg \rightarrow HH$ (left panel) and $gg \rightarrow ZZ$ (right panel), normalized to their exact values.

are normalized to the exact (i.e. unexpanded) leading-order expressions. We see that in both cases, the exact results are reproduced by the high-energy expansion at a level better than 1%, for $\sqrt{s} \gtrsim 750$ GeV. Below this value, the expansion in m_t^2 diverges. In the case of $gg \rightarrow HH$ an expansion to quadratic order in m_H is sufficient, however for $gg \rightarrow ZZ$ a quadratic-order expansion produces a $\sim 1\%$ difference w.r.t. the exact result, which slowly grows with energy. This is resolved by including quartic-order expansion terms. This difference in convergence behaviour can be traced to a factor of $1/m_Z^2$ in the Z-boson polarization sum. Here it is interesting to note that Refs. [28, 29] propose a “hybrid” method in which an expansion is performed in the final-state particle masses, as we discuss here, but the resulting integrals are integrated numerically rather than expanded in the top quark mass. This leads to an easier IBP reduction compared to Ref. [7], which converges on the exact result in a similar way to Fig. 1 (without the divergence of the m_t expansion around $\sqrt{s} \sim 750$ GeV).

4. Padé Approximants

As shown in Fig. 1, the high-energy expansions feature a strong divergence around $\sqrt{s} \approx 750$ GeV when compared to the exact leading-order results. This feature persists at NLO, as can be seen by comparing successive orders in the m_t^2 expansion. Nonetheless, the use of *Padé approximants* can improve the series expansion, providing stable results for significantly smaller values of \sqrt{s} . An $[n/m]$ Padé approximant of some function $f(x)$ is defined as

$$f(x) \approx [n/m](x) = \frac{a_0 + a_1x + a_2x^2 + \dots + a_nx^n}{1 + b_1x + b_2x^2 + \dots + b_mx^m}. \quad (7)$$

The coefficients $a_0, \dots, a_n, b_1, \dots, b_m$ can be fixed by comparing the Taylor series of $[n/m](x)$ around $x \rightarrow 0$ with a series expansion of $f(x)$ to order $n + m$.

Fig. 2 shows Taylor series and Padé approximants of a test function $f(x) = \log(1+x)/(1+x)$. The curves are normalized to $f(x)$. We see that “Padé [4/4]”, in particular, reproduces $f(x)$ extremely well compared to the Taylor series, despite being constructed from a Taylor series to x^8 only. It also reproduces $f(x)$ at the per-mille level for $x < 4$, far beyond the radius of convergence of the Taylor series ($x < 1$).

We construct Padé approximants for the high-energy expansions by replacing $m_t^{2n} \rightarrow m_t^{2n}x^n$ and $m_t^{2n-1} \rightarrow m_t^{2n-1}x^n$, then inserting a numerical value for m_t and building the approximant for

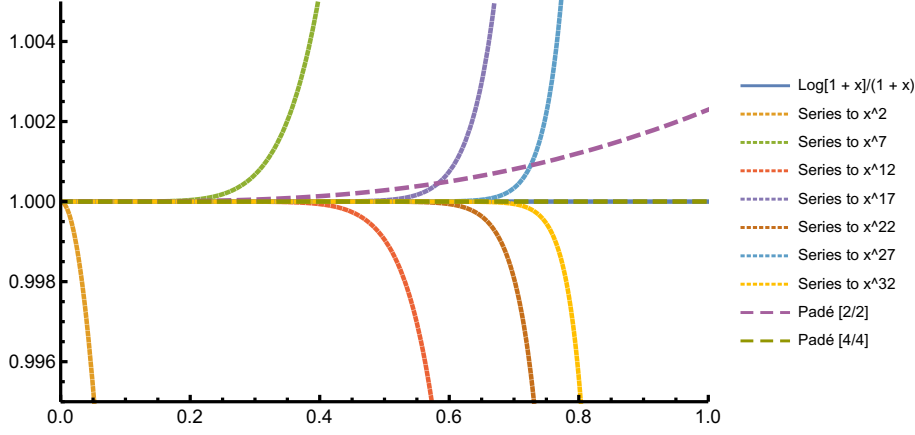


Figure 2: Normalized Taylor series and Padé approximants of a test function $f(x) = \log(1+x)/(1+x)$.

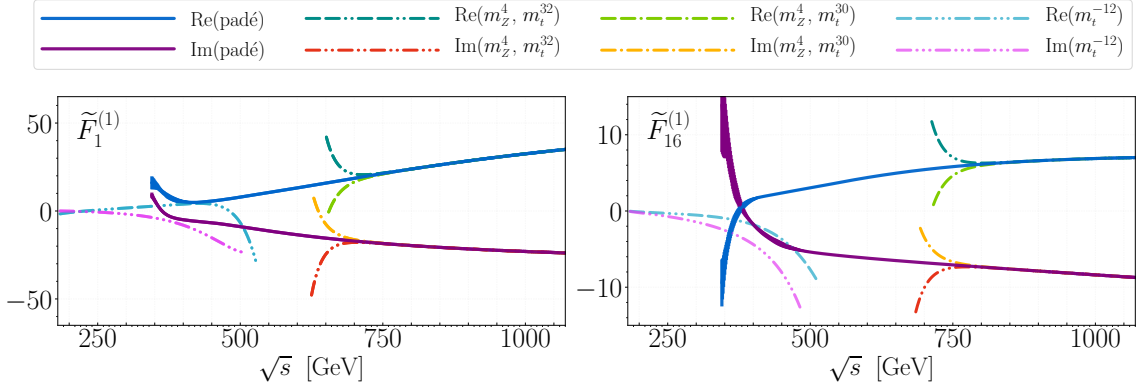


Figure 3: Two NLO form factors of $gg \rightarrow ZZ$. The plots show high-energy expansions and Padé-based approximations, as well the large- m_t expansions. The width of the Padé bands denotes their uncertainty.

$x \rightarrow 0$. Evaluating at $x = 1$ gives the approximated value. In practice, we construct approximations by combining together many different Padé approximants (with different values of n, m), to produce a central value and error estimate. The central value is an average of the Padé approximants, weighted according to three criteria: i) the distance of the nearest pole of the denominator to $x = 1$ in the complex plane, ii) how much input has been used in constructing the approximant, $n + m$, iii) how close to “diagonal” the approximant is, $|n - m|$. In our experience the most reliable approximants are those which use as much input as possible, are close to “diagonal”, and do not have poles close to the evaluation point. Including a collection of “sub-optimal” approximants in this weighted manner, however, leads to better error estimates.

Fig. 3 shows the result of this procedure for two form factors of the NLO $gg \rightarrow ZZ$ amplitude. As in Fig. 1, we see that the m_t^2 expansion diverges for $\sqrt{s} \lesssim 750$ GeV, however the Padé-based approximations discussed above produce stable results for \sqrt{s} values as small as 400 GeV. Fig. 4 shows this procedure applied at the level of NLO virtual-finite cross sections (defined in Eq. (3)) for $gg \rightarrow ZZ$ (left panel) and $gg \rightarrow ZH$ (right panel). The left panel shows that the high-energy expansion, labelled “ m_t^{32}, m_Z^4 ” breaks down around $\sqrt{s} \approx 4m_t$ as usual, and that the Padé-based approximation agrees with the exact numerical evaluation by pySecDec for \sqrt{s} values extending

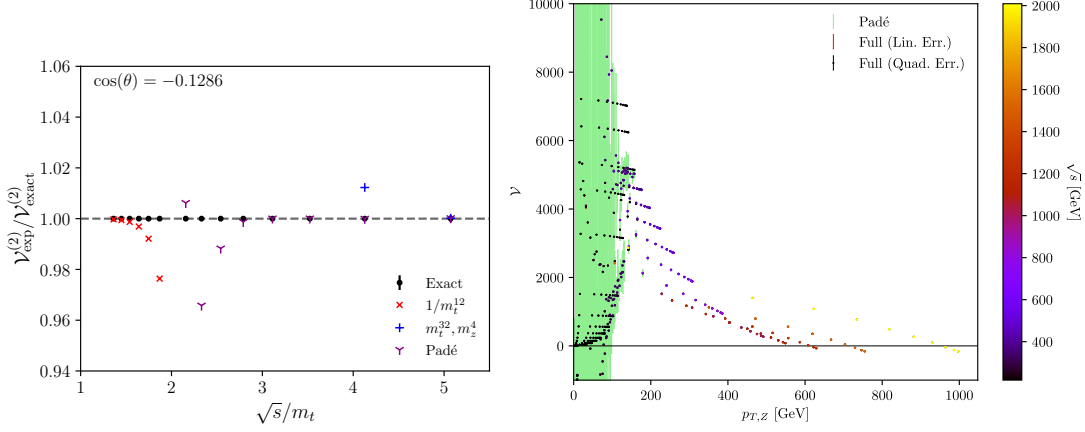


Figure 4: *Left:* (from Ref. [30]) \mathcal{V}_{fin} for $gg \rightarrow ZZ$, normalized to an exact numerical evaluation by `pySecDec`. *Right:* (preliminary¹) \mathcal{V}_{fin} for $gg \rightarrow ZH$, as a function of $p_{T,Z}$. The “Full” points are an evaluation by `pySecDec`, with errors added both linearly and in quadrature when summing the form factors.

below $3m_t$. The right panel shows a comparison for $gg \rightarrow ZH$, as a plot against the Z boson transverse momentum $p_{T,Z}$ rather than \sqrt{s} . We observe that the Padé-based approximation agrees very well with numerical evaluations for all $p_{T,Z} \gtrsim 150$ GeV. Below this value, the error bars of the Padé-based approximation (in green) become enormous. Above this value, the error bars are too small to be seen in the plot.

5. Conclusions

In these proceedings we have discussed the high-energy expansion of $2 \rightarrow 2$ scattering amplitudes, particularly in the context of gluon-fusion processes. We have discussed a method based on Padé approximants which allows the results of the expansion to be improved, thus describing a larger kinematic region than the expansion alone. The high-energy region is computationally expensive to investigate via numerical methods, so an expansion in this region provides valuable input for various approximations. For example, in Ref. [31] information from the high-energy expansion has been combined with numerical evaluations in the rest of the phase space to provide an improved description of the NLO virtual contributions to $gg \rightarrow HH$. Work is on-going to provide a similar combination of complementary information for $gg \rightarrow ZH$.¹

Acknowledgements

The work of JD was partly supported by the Science and Technology Facilities Council (STFC) under the Consolidated Grant ST/T00102X/1.

¹In preparation: Chen, Davies, Heinrich, Jones, Kerner, Mishima, Schlenk, Steihauser (2021/2022)

References

- [1] O.J.P. Eboli, G.C. Marques, S.F. Novaes and A.A. Natale, *TWIN HIGGS BOSON PRODUCTION*, *Phys. Lett. B* **197** (1987) 269.
- [2] E.W.N. Glover and J.J. van der Bij, *HIGGS BOSON PAIR PRODUCTION VIA GLUON FUSION*, *Nucl. Phys. B* **309** (1988) 282.
- [3] T. Plehn, M. Spira and P.M. Zerwas, *Pair production of neutral Higgs particles in gluon-gluon collisions*, *Nucl. Phys. B* **479** (1996) 46 [hep-ph/9603205].
- [4] E.W.N. Glover and J.J. van der Bij, *Z BOSON PAIR PRODUCTION VIA GLUON FUSION*, *Nucl. Phys. B* **321** (1989) 561.
- [5] D.A. Dicus and C. Kao, *Higgs Boson - Z^0 Production From Gluon Fusion*, *Phys. Rev. D* **38** (1988) 1008.
- [6] B.A. Kniehl, *Associated Production of Higgs and Z Bosons From Gluon Fusion in Hadron Collisions*, *Phys. Rev. D* **42** (1990) 2253.
- [7] S. Borowka, N. Greiner, G. Heinrich, S.P. Jones, M. Kerner, J. Schlenk et al., *Full top quark mass dependence in Higgs boson pair production at NLO*, *JHEP* **10** (2016) 107 [1608.04798].
- [8] J. Baglio, F. Campanario, S. Glaus, M. Mühlleitner, M. Spira and J. Streicher, *Gluon fusion into Higgs pairs at NLO QCD and the top mass scheme*, *Eur. Phys. J. C* **79** (2019) 459 [1811.05692].
- [9] J. Grigo, J. Hoff, K. Melnikov and M. Steinhauser, *On the Higgs boson pair production at the LHC*, *Nucl. Phys. B* **875** (2013) 1 [1305.7340].
- [10] J.M. Campbell, R.K. Ellis, M. Czakon and S. Kirchner, *Two loop correction to interference in $gg \rightarrow ZZ$* , *JHEP* **08** (2016) 011 [1605.01380].
- [11] L. Altenkamp, S. Dittmaier, R.V. Harlander, H. Rzehak and T.J.E. Zirke, *Gluon-induced Higgs-strahlung at next-to-leading order QCD*, *JHEP* **02** (2013) 078 [1211.5015].
- [12] A. Hasselhuhn, T. Luthe and M. Steinhauser, *On top quark mass effects to $gg \rightarrow ZH$ at NLO*, *JHEP* **01** (2017) 073 [1611.05881].
- [13] R. Gröber, A. Maier and T. Rauh, *Reconstruction of top-quark mass effects in Higgs pair production and other gluon-fusion processes*, *JHEP* **03** (2018) 020 [1709.07799].
- [14] R. Gröber, A. Maier and T. Rauh, *Top quark mass effects in $gg \rightarrow ZZ$ at two loops and off-shell Higgs boson interference*, *Phys. Rev. D* **100** (2019) 114013 [1908.04061].
- [15] R. Bonciani, G. Degrossi, P.P. Giardino and R. Gröber, *Analytical Method for Next-to-Leading-Order QCD Corrections to Double-Higgs Production*, *Phys. Rev. Lett.* **121** (2018) 162003 [1806.11564].

- [16] L. Alasfar, G. Degrossi, P.P. Giardino, R. Gröber and M. Vitti, *Virtual corrections to $gg \rightarrow ZH$ via a transverse momentum expansion*, *JHEP* **05** (2021) 168 [2103.06225].
- [17] J. Davies, G. Mishima, M. Steinhauser and D. Wellmann, *Double Higgs boson production at NLO in the high-energy limit: complete analytic results*, *JHEP* **01** (2019) 176 [1811.05489].
- [18] J. Davies, G. Mishima, M. Steinhauser and D. Wellmann, *$gg \rightarrow ZZ$: analytic two-loop results for the low- and high-energy regions*, *JHEP* **04** (2020) 024 [2002.05558].
- [19] J. Davies, G. Mishima and M. Steinhauser, *Virtual corrections to $gg \rightarrow ZH$ in the high-energy and large- m_t limits*, *JHEP* **03** (2021) 034 [2011.12314].
- [20] S. Catani, *The Singular behavior of QCD amplitudes at two loop order*, *Phys. Lett. B* **427** (1998) 161 [hep-ph/9802439].
- [21] P. Nogueira, *Automatic Feynman graph generation*, *J. Comput. Phys.* **105** (1993) 279.
- [22] R. Harlander, T. Seidensticker and M. Steinhauser, *Complete corrections of Order α_s to the decay of the Z boson into bottom quarks*, *Phys. Lett. B* **426** (1998) 125 [hep-ph/9712228].
- [23] T. Seidensticker, *Automatic application of successive asymptotic expansions of Feynman diagrams*, in *6th International Workshop on New Computing Techniques in Physics Research: Software Engineering, Artificial Intelligence Neural Nets, Genetic Algorithms, Symbolic Algebra, Automatic Calculation*, 5, 1999 [hep-ph/9905298].
- [24] B. Ruijl, T. Ueda and J. Vermaseren, *FORM version 4.2*, 1707.06453.
- [25] T. van Ritbergen, A.N. Schellekens and J.A.M. Vermaseren, *Group theory factors for Feynman diagrams*, *Int. J. Mod. Phys. A* **14** (1999) 41 [hep-ph/9802376].
- [26] A.V. Smirnov and F.S. Chuharev, *FIRE6: Feynman Integral REduction with Modular Arithmetic*, *Comput. Phys. Commun.* **247** (2020) 106877 [1901.07808].
- [27] G. Mishima, *High-Energy Expansion of Two-Loop Massive Four-Point Diagrams*, *JHEP* **02** (2019) 080 [1812.04373].
- [28] X. Xu and L.L. Yang, *Towards a new approximation for pair-production and associated-production of the Higgs boson*, *JHEP* **01** (2019) 211 [1810.12002].
- [29] G. Wang, Y. Wang, X. Xu, Y. Xu and L.L. Yang, *Efficient computation of two-loop amplitudes for Higgs boson pair production*, *Phys. Rev. D* **104** (2021) L051901 [2010.15649].
- [30] B. Agarwal, S.P. Jones and A. von Manteuffel, *Two-loop helicity amplitudes for $gg \rightarrow ZZ$ with full top-quark mass effects*, *JHEP* **05** (2021) 256 [2011.15113].
- [31] J. Davies, G. Heinrich, S.P. Jones, M. Kerner, G. Mishima, M. Steinhauser et al., *Double Higgs boson production at NLO: combining the exact numerical result and high-energy expansion*, *JHEP* **11** (2019) 024 [1907.06408].